





# Laguerre-Gaussian beam generation via enhanced intracavity spherical aberration

MENG WANG,<sup>1,2,5</sup> YUANYUAN MA,<sup>3,5</sup> QUAN SHENG,<sup>1,2,6</sup>  XI HE,<sup>1,2,4</sup> JUNJIE LIU,<sup>1,2</sup> WEI SHI,<sup>1,2,7</sup> JIANQUAN YAO,<sup>1,2</sup> AND TAKASHIGE OMATSU<sup>3</sup> 

<sup>1</sup>*Institute of Laser and Optoelectronics, School of Precision Instrument and Optoelectronics Engineering, Tianjin University, Tianjin 300072, China*

<sup>2</sup>*Key Laboratory of Optoelectronic Information Science and Technology (Ministry of Education), Tianjin University, Tianjin 300072, China*

<sup>3</sup>*Molecular Chirality Research Center, Chiba University, 1-33 Yayoi-cho, Inage-ku, Chiba 263-8522, Japan*

<sup>4</sup>*Currently at Changchun Institute of Optics, Fine Mechanics and Physics, Chinese Academy of Sciences, Dong\_Nanhu Road 3888, Changchun, Jilin, China*

<sup>5</sup>*These authors contribute equally to this work*

<sup>6</sup>*shengquan@tju.edu.cn*

<sup>7</sup>*shiwei@tju.edu.cn*

**Abstract:** We demonstrate an end-pumped Laguerre-Gaussian (LG) mode-selectable Nd:YVO<sub>4</sub> laser utilizing enhanced intracavity spherical aberration. The cavity was designed to exploit strong spherical aberration generated by an expanded beam, incident on a short-focal-length lens, which enabled oscillation of cavity modes of different order. This compact-cavity laser could operate efficiently with high-order LG mode, with the order of this mode being selectively changed by simply adjusting the distance between the short-focal-length lens and the output coupler. Scalar LG modes from LG<sub>0,±10</sub> to up to LG<sub>0,±33</sub> were observed in the experiment. The output power of the LG<sub>0,±33</sub> mode was 1.87 W under an absorbed pump power of 6.6 W.

© 2021 Optical Society of America under the terms of the [OSA Open Access Publishing Agreement](#)

## 1. Introduction

Lasers emitting Laguerre-Gaussian (LG) modes which feature hollow intensity profile and non-zero orbital angular momentum (OAM) are of intense interest for applications such as material processing, optical communication, and optical trapping [1,2]. LG beams can be obtained using a number of approaches. Some of the approaches which have been demonstrated include using external-cavity devices including holograms or cylindrical lens pairs to transform a Hermite-Gaussian beam into a LG beam, or through intracavity means, whereby intracavity components are utilized to preferentially oscillate modes within a laser resonator [1,2]. In comparison to external-cavity approaches, intracavity approaches typically yield superior power handling, beam quality and conversion efficiency (when additional processes such as non-linear conversion take place) [3]. Essential to directly generating an LG laser beam from a laser resonator is to introduce mode-varying laser gain or cavity loss, so that the net gain of a desired order of LG mode is different to that of the “fundamental”, Gaussian (TEM<sub>0,0</sub>) mode, and other undesired LG modes. This can be thought of as tailoring the laser cavity characteristics such that mode competition does not take place. There have been a number of methods demonstrated to achieve this, including use of a defect spot on a cavity mirror [4,5], using a pump beam with a ring intensity profile [6–8], introducing natural or thermally induced birefringence [9–11], and host of other intracavity mode-selecting devices [1,12]. A critical aspect of these approaches is that the cavity in which these techniques are applied, can oscillate both high-order LG and Hermite-Gaussian (HG) modes [13].

One approach which is particularly interesting is the application of spherical aberration to facilitate selection of intracavity modes with hollow intensity profile [3,14–16]. Spherical aberration is typically a characteristic of spherical lenses, wherein the focal position of rays vary as they are incident across the lenses aperture. Spherical aberration is typically undesirable in a laser cavity since it may distort the beam and decrease the lasers efficiency. However, with mode selection in mind, strong spherical aberration in the cavity can be advantageous. Given the intracavity size of the  $TEM_{0,0}$  mode is smaller than that of high-order LG modes, mode differentiation by exploiting spherical aberration becomes possible. In 2009, Senatsky *et al.* demonstrated an end-pumped 1030 nm Yb:YAG laser which produced an incoherent multi-mode circular beam, by using intracavity spherical aberration [14]. In their later work, they altered their cavity (extending it to over 80 cm) to narrow the cavity stability region for certain modes, to produce laser output in a single high-order LG mode [15,16].

To generate high power laser output which has a pure, high-order LG mode profile, it is necessary to ensure that the desired LG mode is well distinguished from other modes within the laser cavity. This can be achieved by enhancing the net gain difference between a desired LG mode and its neighboring modes. Within the literature, lasers generating LG mode output based on spherical aberration can generate a single-mode LG beam only when long cavities are used, and this narrows the “operating zone” of each LG mode [3,15,16]. In this work, we present a LG mode laser based on enhanced spherical aberration. Key to this approach is inducing strong spherical aberration within the cavity via expansion of the intracavity mode and having it incident on an intracavity, short-focal-length spherical lens. This ensures that the optical path of the different orders of transverse modes with different spot sizes are spatially separated. A mirror is then positioned near the focal plane of the short-focal-length lens to preferentially provide feedback to the desired mode (by virtue of varying its distance from the lens). This is the means by which mode selection is achieved. In this work, we apply this concept to demonstrate an end-pumped a-cut Nd:YVO<sub>4</sub> laser which delivers multi-watt high-order scalar LG mode output with LG mode selectability. The highest order hollow-intensity profile LG mode which could be selectively generated from this laser was  $LG_{0,\pm 33}$ .

## 2. Experimental arrangement

The experimental setup of the LG mode laser is shown in Fig. 1(a). The pump source was a fiber-coupled, wavelength-stabilized laser diode at 878.6 nm. The pump light delivered from the fiber with a diameter of 200  $\mu\text{m}$  and a NA of 0.14 was reimaged (to a spot of radius of  $\sim 120 \mu\text{m}$ ) into an a-cut Nd:YVO<sub>4</sub> crystal by two focusing lenses. The 0.5-at.-%-doped Nd:YVO<sub>4</sub> crystal with dimensions of  $3 \times 3 \times 5 \text{ mm}^3$  was coated anti-reflection (AR) at both 878.6 nm and 1064 nm, and absorbs  $\sim 61\%$  of the incident unpolarized pump light. The thermal focal length in the crystal was estimated to be  $\sim 140 \text{ mm}$  under the maximum pump power used in the experiment of 10.9 W; this value was derived assuming a fractional thermal load of 17.4% under lasing at 1064 nm and using the Eq. (13) in reference [17]. The laser cavity consisted of a plano-concave input mirror M1, a flat output coupler M2, and two intracavity lenses L1 (BK7, plano-convex) and L2 (BK7, plano-convex) with focal lengths of 150 mm and 33.9 mm, respectively. M1 was coated high-reflecting (HR) at 1064 nm on one side and AR at 878.6 nm on both sides. Both L1 and L2 were coated for AR at 1064 nm, and M2 had a transmittance of 10% at 1064 nm. The input mirror M1 had a small radius of curvature of 50 mm, which helped to keep an almost constant, small ( $\sim 90 \mu\text{m}$ )  $TEM_{0,0}$  beam radius at the laser crystal, which was relatively insensitive to the changing thermal focal length of the crystal, under different incident pump power. Similarly, the beam size at the lens L1 also remained largely constant.

The Nd:YVO<sub>4</sub> crystal was placed very close to M1 (a distance of  $\sim 1 \text{ mm}$ ). The distance between the crystal and L1 (marked as  $d_1$ ) was 155 mm, while that between lens L2 and the  $T=10\%$  output coupler M2 (marked as  $d_3$ ) was close to the focal length of L2. With this setup,

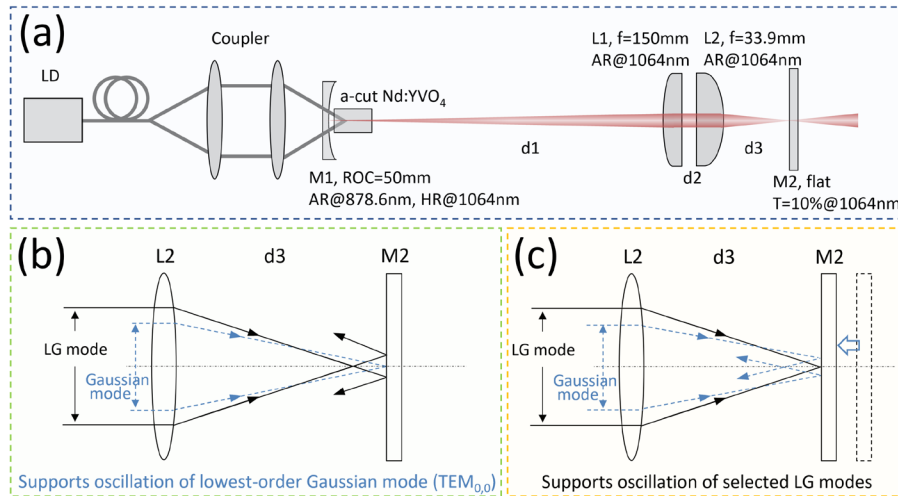


**Fig. 1.** Schematic of the (a) experimental setup, and mode-selection of (b) the Gaussian mode with smaller beam size and (c) the LG modes with larger beam size.

the laser beam was collimated between the lenses L1 and L2, so that the distance between L1 and L2 (marked as  $d_2$ ) would have little influence on the beam propagation. In the experiment,  $d_2$  was set to  $\sim 20$  mm. The output coupler M2 was mounted on a micrometer-resolution translation stage, so that the distance  $d_3$  could be carefully adjusted. The total cavity length was  $\sim 225$  mm, which was significantly shorter than that used to generate single high-order mode operation in former spherical-aberration-based works [3,15,16].

In this setup, given that the intracavity TEM<sub>0,0</sub> mode has a small beam radius of  $\sim 90$   $\mu\text{m}$  or a little lower (depending on the induced thermal lens) at the Nd:YVO<sub>4</sub> crystal, the beam radius expands significantly to  $\sim 600$   $\mu\text{m}$  or larger at the lens L1. For the high-order LG <sub>$p,m$</sub>  modes, the beam radii  $W_{p,m}$  will be much larger than that of the TEM<sub>0,0</sub> mode given the equation [3].

$$W_{pm} = w_0(2p + |m| + 1)^{1/2} \quad (1)$$

where  $w_0$  is the TEM<sub>0,0</sub> beam radius. When the collimated beam with such large size was focused by the short-focal-length spherical lens L2, the spherical aberration is very strong. Here, the focal point of the rays at the edge of the beam deviate significantly from that of the central rays, because of the strong spherical aberration. For a laser beam to resonate within this cavity, its focal point (or beam waist) should be exactly on the flat reflective surface of M2. Therefore, when the distance  $d_3$  equals that of the focal position of rays passing through the central part of L2, these central rays are fed back, while rays toward the edge of the lens are reflected out of the cavity. This supports the oscillation of the TEM<sub>0,0</sub> mode, as shown in Fig. 1(b). If  $d_3$  is a bit smaller than the case above, so that edge rays come to focus on M2, the TEM<sub>0,0</sub> mode would suffer loss higher than that of the edge rays, and force the laser to operate in a hollow LG resonant mode, as shown in Fig. 1(c). With the output coupler M2 closer to the lens L2, the actual focal point of higher-order of LG mode (with larger ring-diameter on the lens L2) will be on the M2, and make the corresponding mode oscillating.

With the short-focal-length lens L2 in the cavity, the stability zone of the fundamental mode and the “operating zone” of each LG mode in terms of the distance  $d_3$  became quite narrow. Meanwhile, the strong spherical aberration induced by the expanded beam (through L1) and the short-focal-length lens L2 made the light paths of the different modes well differentiated. By adjusting the distance  $d_3$ , we were able to control the cavity feedback for the different modes and

achieve mode selection. Plotted in Fig. 2(a) is the calculated  $TEM_{0,0}$  beam radius throughout the cavity. Note that the beam sizes of the high-order LG modes at each spatial position within the cavity can be calculated using Eq. (1), and are several times larger than that of the  $TEM_{0,0}$  mode. Figure 2(b) shows the calculated deviation in focal position of edge rays to central rays, as a function of beam radius. It can be seen that the deviation is  $\sim 1.9$  mm with a beam radius of 3.5 mm. One may interpret these values as follows; considering the  $\sim 600$   $\mu m$   $TEM_{0,0}$  mode radius, if we targeted oscillation of the  $LG_{0,\pm 33}$  mode (i.e.  $p=0$  and  $m=\pm 33$ ), a beam with radius 3.5 mm would be produced, incident on L2. To ensure oscillation of this  $LG_{0,\pm 33}$  mode, the output coupler M2 must be moved toward L2 by a distance of 1.9 mm from the location which supports oscillation of the  $TEM_{0,0}$  mode.

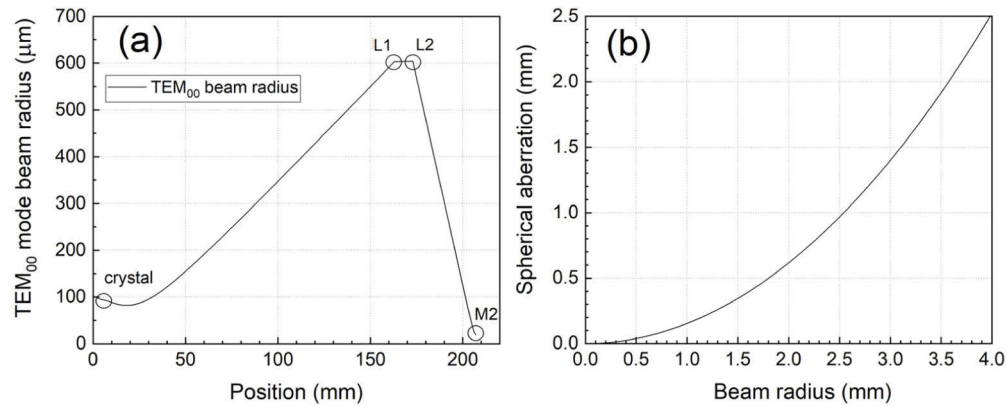


**Fig. 2.** (a) The fundamental mode beam size (radius) in the cavity and (b) lateral displacement of focal point owing to the spherical aberration of the  $f=33.9$  mm BK7 plano-convex lens L2 as a function of beam radius.

### 3. Experimental results and discussion

The output coupler M2 was first positioned to generate the  $TEM_{0,0}$  mode, i. e., at the actual focal point of the central rays, under an incident pump power of 1.03 W. M2 was then progressively translated toward the lens L2 (in effect decreasing the distance  $d_3$ ), and this led to the oscillation of hollow modes as expected. We use  $\delta$  to represent the distance that the output coupler M2 is moved toward L2, from its original position (i.e.  $\delta=0$  which generates the  $TEM_{0,0}$  mode). Shown in Fig. 3 are intensity profiles of a range of mode outputs generated from the system. The beam intensity profiles were recorded using a CCD camera (Ophir SP907), at different  $\delta$  and under a fixed incident LD pump power of 1.03 W. It can be seen that the hollow profiles were the superpositions of doughnut-like and petal-like beams when  $\delta$  was less than 1.30 mm. When  $\delta$  was larger, the beam profiles were clearly petal-like.

By observing the near-field and far-field beam profiles, we found that the oscillating hollow beams were superpositions of multiple modes which contained different angular indices  $|m|$  (near-field and far-field beam profiles were different) when the  $\delta$  was less than 1.30 mm. The laser became propagation-invariant and clearly petal-like when  $\delta$  was greater than 1.30 mm, which revealed that the LG beam contained only one angular indices  $|m|$ . The petal-like pattern was resulted from the coherent coupling of doughnut  $LG_{0,+m}$  and  $LG_{0,-m}$  modes. By counting the petals, we can verify the order of the LG modes. The lowest order of single- $|m|$  mode emission generated from the system was  $LG_{0,\pm 10}$  with  $\delta=1.30$  mm, while the highest order of mode generated was  $LG_{0,\pm 33}$  with  $\delta=1.80$  mm. The laser stopped oscillating for larger values of

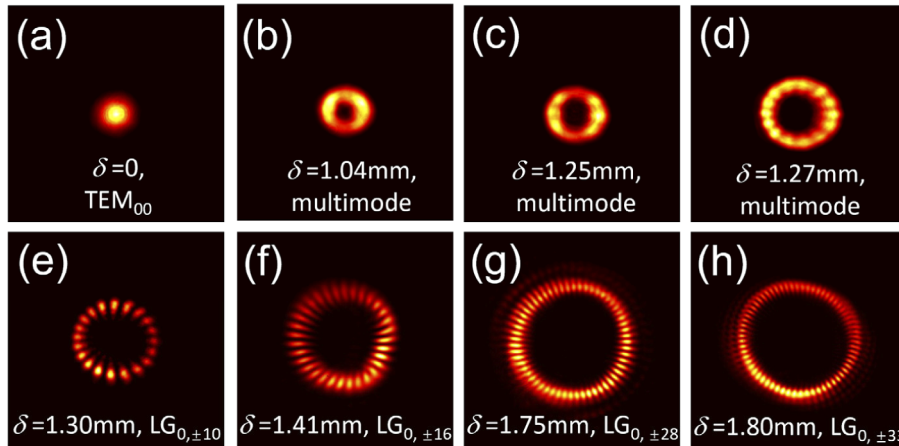


**Fig. 3.** The near-field beam patterns with different  $\delta$  under 1.03 W incident pump power. (a)  $\delta=0$ ,  $P_{\text{out}}=0.256$  W; (b)  $\delta=1.09$  mm,  $P_{\text{out}}=0.261$  W; (c)  $\delta=1.25$  mm,  $P_{\text{out}}=0.255$  W; (d)  $\delta=1.27$  mm,  $P_{\text{out}}=0.236$  W; (e)  $\delta=1.30$  mm,  $P_{\text{out}}=0.191$  W; (f)  $\delta=1.41$  mm,  $m=\pm 16$ ,  $P_{\text{out}}=0.057$  W; (g)  $\delta=1.75$  mm,  $m=\pm 28$ ,  $P_{\text{out}}=0.030$  W; (h)  $\delta=1.80$  mm,  $m=\pm 33$ ,  $P_{\text{out}}=0.018$  W.

$\delta$ . These results demonstrate how easily and controllably, a broad range of high-order LG modes can be selectively generated using spherical aberration, within a compact cavity arrangement.

Figure 4 shows the power transfer characteristics of the laser with different  $\delta$ , as well as corresponding beam profiles generated at the maximum incident pump power of 10.8 W (6.6 W absorbed). In each of these cases, the laser output power increased linearly with the incident

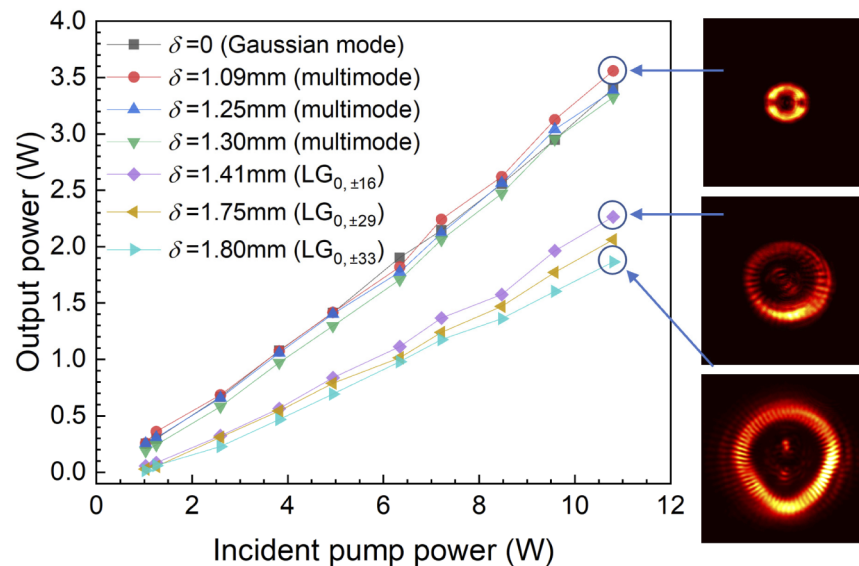


**Fig. 4.** Plotted are the power transfer characteristics of the laser when operating with a range of  $\delta$  (as detailed in the plot key). The spatial beam profiles are shown for the case when the laser was operating at  $\delta=1.09$  mm (multimode),  $\delta=1.41$  mm (initially  $LG_{0,\pm 16}$ ) and  $\delta=1.80$  mm (initially  $LG_{0,\pm 33}$ ), under the maximum incident pump power of 10.8 W. The lines are a guide to the eye.



pump power. The output power with  $\delta$  set to 0, 1.09 mm, 1.25 mm, 1.30 mm, 1.41 mm, 1.75 mm and 1.80 mm were 3.41 W, 3.56 W, 3.38 W, 3.33 W, 2.27 W, 2.06 W and 1.87 W, respectively. The maximum optical efficiency was 33.0%, while the conversion efficiency in terms of the absorbed pump power reached 53.9%. The conversion efficiency from the absorbed pump to the highest order of mode  $LG_{0,\pm 33}$  output was 28.3%. We did not further increase the pump power due to risk of component damage, especially as the beam size on the output coupler M2 was quite small (the  $TEM_{0,0}$  mode radius here is  $\sim 20 \mu\text{m}$ ).

It is interesting to note that the low-order ( $m < 20$ ) LG modes produced from the system evolved to include multiple modes, when pumped at high powers and producing watt-level output. The far-field profiles exhibited structure comprising multiple-modes, while the near-field profiles remained hollow. Using lens L2 with stronger spherical aberration to further differentiate the optical path of different modes was effective at overcoming this characteristic when operating at high pump power. For high-order LG modes with  $m > 20$ , since the spherical aberration induced focal point displacement between the neighboring modes was larger, the multimode operation observed for  $m < 20$  did not occur. However, the astigmatic thermal lens within the Nd:YVO<sub>4</sub> crystal broke the cylindrical symmetry of the cavity and degrade the beam quality of the generated LG modes [18]. It can be seen in the inset of Fig. 4 that some Ince-Gaussian-like components emerged near the center of the beams. The polarization of the laser output was always observed to be parallel to the c-axis of the a-cut Nd:YVO<sub>4</sub> crystal, and hence the generated LG modes were scalar.

The lower output power (conversion efficiency) of high-order modes ( $LG_{0,\pm 16}$ ,  $LG_{0,\pm 29}$  and  $LG_{0,\pm 33}$ ) compared with those of the low-order multi modes was due to the mismatch between the incident pump beam profile and the beam profile of the oscillating mode. The pump beam radius was  $\sim 120 \mu\text{m}$  and the calculated  $TEM_{0,0}$  mode radius in the crystal was  $\sim 90 \mu\text{m}$ . For the high-order modes, from Eq. (1) we know the beam sizes were much larger than that of the pump beam. In this situation, the hollow intensity profiles can not fully extract the population inversion, and resulted in the decreased conversion efficiency as well as the increased laser threshold. We therefore expect that even higher-order modes can be generated with dynamic optimization of the pump beam diameter to better mode-match with the larger high-order LG modes, and the use of both larger  $\delta$  and higher incident pump power.

We believe that the petal-like beam profiles above are a result of coherent coupling of  $LG_{0,+m}$  and  $LG_{0,-m}$  modes which are generated within the system. These modes are indifferently generated as a result of perturbations which may include astigmatism, environmental vibrations of resonator components, thermal lensing and relaxation oscillations. A similar characteristic was also observed in Ref. [19]. In the experiment, we also tried to force the handedness of our generated LG modes by inserting an etalon in the laser cavity and by misaligning the cavity mirrors a little [20,21]. However, since the focusing lens and the mirror near its focal point formed a “cat-eye” retroreflector, the light from any angle of incidence is reflected back, and the laser keeps oscillating without “seeing” any obvious misalignment [22]. As a result, it is difficult to preferentially oscillate either the  $LG_{0,+m}$  or  $LG_{0,-m}$  mode. As shown in Fig. 5(a), before breaking the cylindrical symmetry with the tilted etalon, the pattern before the cylindrical lens was clearly petal-like and intensities of the two strokes of the x-shaped pattern after the cylindrical lens were similar, which indicates the  $LG_{0,+29}$  and  $LG_{0,-29}$  modes have similar intensities. With the etalon in the cavity, the two strokes of the x-shaped pattern became much different, as shown in Fig. 5(b), reveals that one of the two handedness was much weaker, but can not be eliminated. Meanwhile, the petal-like pattern became less clear. The development of an effective means of differentiating the handedness of the LG mode output forms the basis of our continued work in this area.

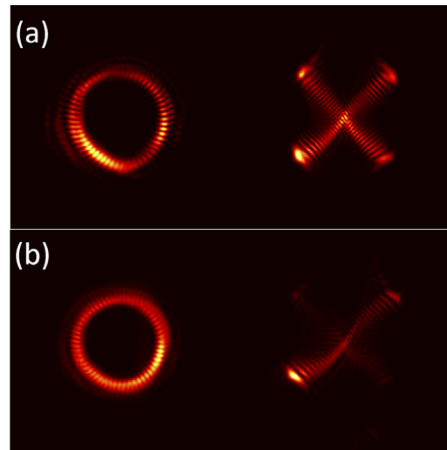


**Fig. 5.** The beam profiles of the  $LG_{0, \pm 29}$  mode without (a) and with (b) the intracavity etalon, before and after being focused by a cylindrical lens.

#### 4. Conclusion

In conclusion, we have demonstrated a laser which can selectively output LG modes of different order, with hollow intensity profile, by implementing enhanced intracavity spherical aberration. Beam expansion in conjunction with a short-focal-length lens inside the laser cavity was used to induce strong spherical aberration, which enabled differentiation of LG modes within the cavity. Mode selection was achieved with precise positioning of the laser cavity output coupler, relative to the short-focal-length lens. This compact system was able to efficiently generate multi-watt LG mode output, with high-order modes up to  $LG_{0, \pm 33}$ .

**Funding.** National Natural Science Foundation of China (61975146, 62075159); Major Scientific and Technological Innovation Projects of Key R&D Plans in Shandong Province (2019JZZY020206); KAKENHI Grants-in-Aid of the Japan Society for the Promotion of Science (JP18H03884); Core Research for Evolutional Science and Technology (JPMJCR1903).

**Disclosures.** The authors declare no conflicts of interest.

**Data availability.** Data underlying the results presented in this paper are not publicly available at this time but may be obtained from the authors upon reasonable request.

#### References

1. A. Forbes, "Structured light from lasers," *Laser Photonics Rev.* **13**(11), 1900140 (2019).
2. T. Omatsu, K. Miyamoto, and A. J. Lee, "Wavelength versatile optical vortex lasers," *J. Opt.* **19**(12), 123002 (2017).
3. Y. Senatsky, J. F. Bisson, J. Li, A. Shirakawa, M. Thirugnanasambandam, and K. Ueda, "Laguerre-Gaussian modes selection in diode-pumped solid-state laser," *Opt. Rev.* **19**(4), 201–221 (2012).
4. A. Ito, Y. Kozawa, and S. Sato, "Generation of hollow scalar and vector beams using a spot-defect mirror," *J. Opt. Soc. Am. A* **27**(9), 2072–2077 (2010).
5. A. J. Lee, T. Omatsu, and H. M. Pask, "Direct generation of a first-Stokes vortex laser beam from a self-Raman laser," *Opt. Express* **21**(10), 12401–12409 (2013).
6. J.-F. Bisson, Y. Senatsky, and K.-I. Ueda, "Generation of Laguerre-Gaussian modes in Nd:YAG laser using diffractive optical pumping," *Laser Phys. Lett.* **2**(7), 327–333 (2005).
7. Y. Zhao, Q. Liu, W. Zhou, and D. Shen, "~1 mJ pulsed vortex laser at 1645 nm with well-defined helicity," *Opt. Express* **24**(14), 15596–15602 (2016).
8. Y. Ma, A. J. Lee, H. M. Pask, K. Miyamoto, and T. Omatsu, "Direct generation of 1108 nm and 1173 nm Laguerre-Gaussian modes from a self-Raman Nd:GdVO<sub>4</sub> laser," *Opt. Express* **28**(16), 24095–24103 (2020).
9. K. Yonezawa, Y. Kozawa, and S. Sato, "Generation of a radially polarized laser beam by use of the birefringence of a c-cut Nd:YVO<sub>4</sub> crystal," *Opt. Lett.* **31**(14), 2151–2153 (2006).
10. A. Ito, Y. Kozawa, and S. Sato, "Selective oscillation of radially and azimuthally polarized laser beam induced by thermal birefringence and lensing," *J. Opt. Soc. Am. B* **26**(4), 708–712 (2009).

11. C.-H. Chuang, C.-Y. Ho, Y.-C. Hsiao, C.-P. Chiu, and M.-D. Wei, "Selection rule for cavity configurations to generate cylindrical vector beams with low beam quality factor," *Opt. Express* **29**(4), 5043–5054 (2021).
12. D. Lin, J. M. O. Daniel, and W. A. Clarkson, "Controlling the handedness of directly excited Laguerre–Gaussian modes in a solid-state laser," *Opt. Lett.* **39**(13), 3903–3906 (2014).
13. J. C. Tung, Y. H. Hsieh, T. Omatsu, K. F. Huang, and Y. F. Chen, "Generating laser transverse modes analogous to quantum Green's functions of two-dimensional harmonic oscillators," *Photonics Res.* **5**(6), 733–739 (2017).
14. Y. Senatsky, J.-F. Bisson, A. Shelobolin, A. Shirakawa, and K. Ueda, "Circular modes selection in Yb:YAG laser using an intracavity lens with spherical aberration," *Laser Phys.* **19**(5), 911–918 (2009).
15. M. P. Thirugnanasambandam and Y. Senatsky, "Generation of very-high order Laguerre-Gaussian modes in Yb:YAG ceramic laser," *Laser Phys. Lett.* **7**(9), 637–643 (2010).
16. M. P. Thirugnanasambandam, Y. Senatsky, A. Senatsky, and K. Ueda, "Multi-ring modes generation in Yb:YAG ceramic laser," *Opt. Mater.* **33**(5), 675–678 (2011).
17. M. E. Innocenzi, H. T. Yura, C. L. Fincher, and R. A. Fields, "Thermal modeling of continuous-wave end-pumped solid-state lasers," *Appl. Phys. Lett.* **56**(19), 1831–1833 (1990).
18. D. Sun, H. Lin, J. Guo, W. Wang, and X. Liang, "Sub-100 W TEM<sub>00</sub> bulk Nd:GdVO<sub>4</sub> oscillator based on orthogonal thermal compensation," *Opt. Lett.* **43**(18), 4346–4349 (2018).
19. Y. F. Chen and Y. P. Lan, "Dynamics of helical-wave emission in a fiber-coupled diode end-pumped solid-state laser," *Appl. Phys. B* **73**(1), 11–14 (2001).
20. Y. Chen, M. Ding, J. Wang, L. Wang, Q. Liu, Y. Zhao, Y. Liu, D. Shen, Z. Wang, X. Xu, and V. Petrov, "High-energy 2  $\mu$ m pulsed vortex beam excitation from a Q-switched Tm:LuYAG laser," *Opt. Lett.* **45**(3), 722–725 (2020).
21. J. Kim and J. W. Kim, "Direct generation of an optical vortex beam in a single-frequency Nd:YVO<sub>4</sub> laser," *Opt. Lett.* **40**(3), 399–402 (2015).
22. Z. Xu, S. Zhang, Y. Li, and W. Du, "Adjustment-free cat's eye cavity He-Ne laser and its outstanding stability," *Opt. Express* **13**(14), 5565–5573 (2005).